Elsevier Editorial System(tm) for Electrochimica Acta

Manuscript Draft

Manuscript Number:

Title: Nanoceria Acting as Oxygen Reservoir for Biocathodes in Microbial Fuel cells

Article Type: Research Paper

Keywords: Microbial fuel cells, Biocathodes, Nanoceria, Microbial catalysis, Sm-doped CeO2 nanoparticles

Corresponding Author: Dr. Pierangela Cristiani, M.S.

Corresponding Author's Institution: RSE - Ricerca Sul Sistema Energetico

First Author: Stefania Marzorati, PhD

Order of Authors: Stefania Marzorati, PhD; Pierangela Cristiani, M.S.; Mariangela Longhi, PhD; Stefano P Trasatti, PhD; Enrico Traversa, PhD

Abstract: High materials costs and low performance of microbial fuel cells (MFCs) are the persisting bottlenecks that significantly affect their applications. In membraneless single-chamber MFCs using carbon-based electrodes and an air-breathing cathode, bacteria play a role for both the anodic and cathodic processes. However, the microbial cathodic semi-reaction is the rate-determining step that can impair the advantage of the natural availability of oxygen in air. In this work, the microbial catalysis was improved adding cerium oxide nanoparticles (nanoceria) in carbon-based cathodes of air-breathing MFCs, boosting their performance. Two kinds of nanoparticles were tested: CeO2 and Sm-doped CeO2 (Sm-CeO2) on carbon powder, using pristine carbon powder cathodes as a control. The power generated was 113, 65 and 31 mWh m-2, for Sm-CeO2, CeO2 and control MFCs, respectively, during four subsequent fed cycles of 0.036 mol L-1 Na-acetate in carbonate buffer solution. The better performance of MFCs was correlated to the oxygen preferential and controlled entrapping and release via Ce4+/3+ redox reaction at the carbon particle surface, as well as to the increased cathode active specific surface area. The achieved results suggest that nanoceria can act as oxygen storage for bacteria in the anaerobic biofilm colonizing the cathode.

Milan, 23 February 2019

Dear Scientific Committee of Electrochimica Acta,

It is my pleasure to submit to Your attention the manuscript entitled: " ***Nanoceria Acting as Oxygen Reservoir for Biocathodes in Microbial Fuel cells***" to be considered for publication as an original research article.

The work presents and discusses a simply and cost-effective catalyst to solve the issue related to the unsatisfactory performance of carbon based biocathodes of microbial fuel cells (MFCs), that actually limits promising real applications of these systems.
Mostly important, nanoceria is demonstrated able to boost microbial cathodes of membraneless MFCs, showing in this way that this catalyst is not toxic, on the contrary, it actually stimulates the metabolism of the bacteria pool active in the bioelectrochemical system studied.
The paper discusses the mechanism of nanoceria action, creating an oxygen reservoir inside the biocathode.
This effect was correlated to the preferential and controlled entrapping and release of oxygen via $Ce^{4+/3+}$ redox reaction at the carbon particle surface, as well as to the increasing cathode active surface.
The achieved advantage in terms of microbial fuel cell power were relevant with respect the control and these performances are expected to be superior in future with more optimized electrodes than the ones used for this preliminary experimentation.
This fact open the possibility of further improvement of our results, when nanoceria will be applied to more optimized systems.

The publication is approved by all the authors and by the responsible authorities where the work has been carried out.

I can confirm with the other authors that each of us approve the version of the manuscript and that there are no conflict of interest, including any financial, personal or other relationships with other people or organizations within three years of beginning the submitted work that could inappropriately influence, or be perceived to influence, our work.

Hoping in a positive response, and thanking for Your consideration,
I look forward to the challenge of publishing this article with the journal.

Truly
Pierangela Cristiani

Pierangela Cristiani
RSE - Ricerca sul Sistema Elettrico S.p.A.,
Sustainable Development and Energy Source Department
Via Rubattino 54, 20134 Milan, Italy
Tel./fax: +390239924655/4608, *pierangela.cristiani@rse-web.it*

Higlights

- Nanoceria boosts ORR in biocathodes of air-breathing single chamber MFCs
- An oxygen reservoir is created inside the microbial cathodes by CeO_2
- The oxygen reservoir stimulates bacterial metabolism in the MFC system
- The role played by the Ce redox couple results to be minor

Graphical Abstract (for review)

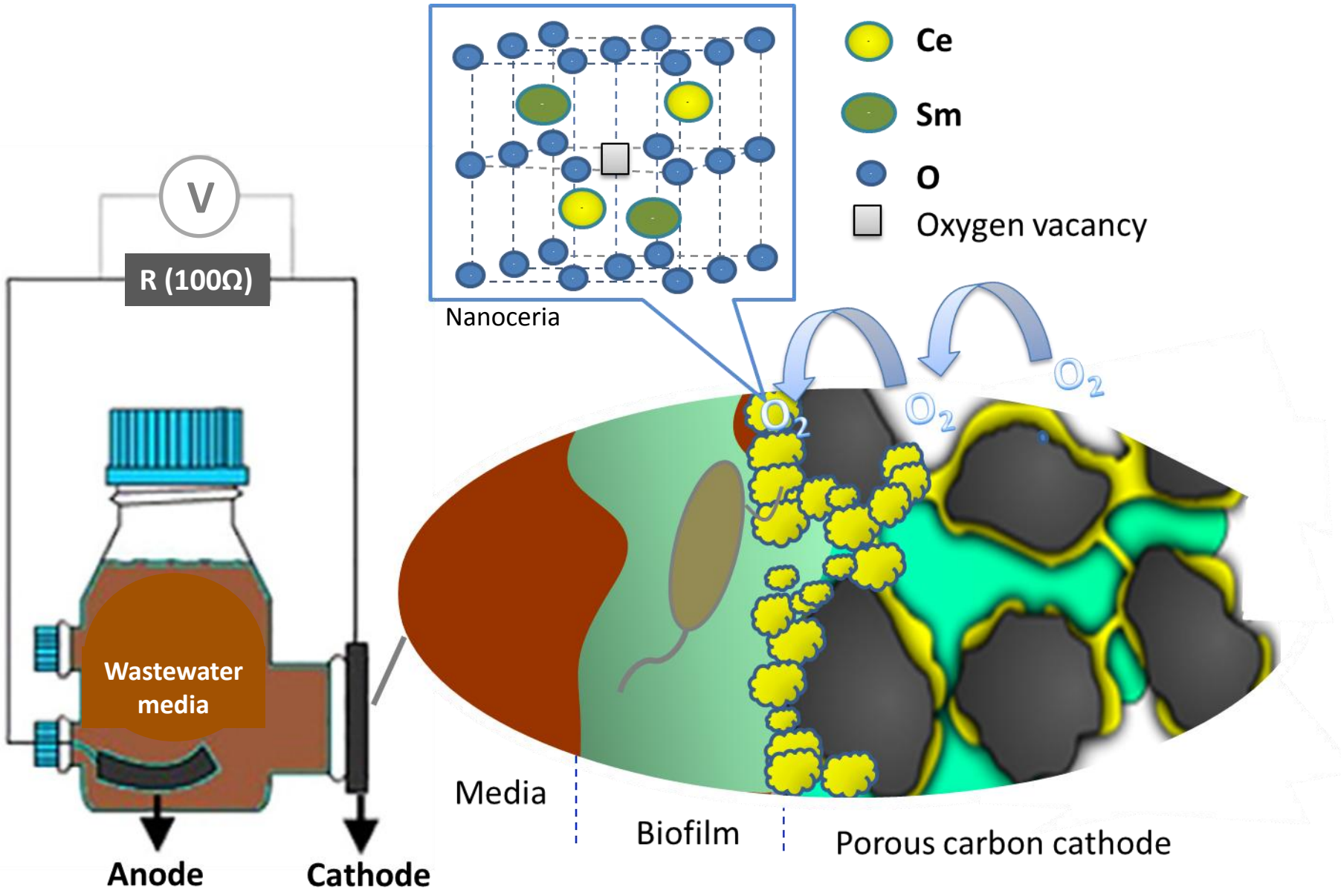

Nanoceria Acting as Oxygen Reservoir for Biocathodes in Microbial Fuel cells

Stefania Marzorati,[a] Pierangela Cristiani,[*b] Mariangela Longhi,[c] Stefano P. Trasatti [a] and Enrico Traversa[*d]

[a.]Department of Environmental Science and Policy - Università degli Studi di Milano, via Celoria 2, 20133 Milano, Italy.

[b.] Ricerca sul Sistema Elettrico – RSE SpA, Sustainable Development and Energy Sources Department, Via Rubattino 54, 20134 Milano, Italy. E-mail: Pierangela.Cristiani@rse-web.it

[c.]Dipartimento di Chimica - Università degli Studi di Milano, via Golgi 19, 20133 Milano, Italy.

[d.]School of Materials and Energy, University of Electronic Science and Technology of China, 2006 Xiyuan Road, Chengdu 611731, Sichuan, China. E-mail: traversa@uestc.edu.cn

*Corresponding authors: Pierangela Cristiani and Enrico Traversa

Keywords

Microbial fuel cells, Biocathodes, Nanoceria, Microbial catalysis, Sm-doped CeO_2 nanoparticles

Abstract

High materials costs and low performance of microbial fuel cells (MFCs) are the persisting bottlenecks that significantly affect their applications. In membraneless single-chamber MFCs using carbon-based electrodes and an air-breathing cathode, bacteria play a role for both the anodic and cathodic processes. However, the microbial cathodic semi-reaction is the rate-determining step that can impair the advantage of the natural availability of oxygen in air. In this work, the microbial catalysis was improved adding cerium oxide nanoparticles (nanoceria) in carbon-based cathodes of air-breathing MFCs, boosting their performance. Two kinds of nanoparticles were tested: CeO_2 and Sm-doped CeO_2 (Sm-CeO_2) on carbon powder, using pristine carbon powder cathodes as a control. The power generated was 113, 65 and 31 mWh m^{-2}, for Sm-CeO_2, CeO_2 and control MFCs, respectively, during four subsequent fed cycles of 0.036 mol L^{-1} Na-acetate in carbonate buffer solution. The better performance of MFCs was correlated to the oxygen preferential and controlled entrapping and release *via* $Ce^{4+/3+}$ redox reaction at the carbon particle surface, as well as to the increased cathode active specific surface area. The achieved results suggest that nanoceria can act as oxygen storage for bacteria in the anaerobic biofilm colonizing the cathode.

1. Introduction

The microbial fuel cell technology has been attracting a great scientific interest over the last decade, especially for its potential in recovering organic pollutants from wastewater [1]. In a MFC, the bacteria can catalyse one or both the red-ox semi-reactions, producing electricity directly from the degradation of organic diluted wastes [1–6]. In a broader context, microbial bioelectrochemical systems promise revolutionary advantages also for soil and sediments bioremediation [7], innovation in robotics [8] and for healthcare applications [9] as well as for energy recovering purpose. However, the deployment of bioelectrochemical technologies is still hindered by several weaknesses and in particular: i) low cathodic kinetics in neutral media; ii) poor performance in harsh working conditions; iii) the utilization of effective, but economically unsustainable chemical catalysts such as platinum group metal (PGM).

In recent studies, membraneless single-chamber MFCs using an air breathing cathode have been extensively investigated as one of the most promising cost-effective system [1,10–13]. In this configuration, bacteria build biofilms on both the electrodes playing several paramount roles: i) promote the oxidation of fuel (biodegradable organics) at the anode; ii) enhance the oxygen reduction reaction (ORR) at the cathode, in an environment rich of organic by-products or sulphides where PGM catalysts would be poisoned; iii) consume the oxygen and prevent its diffusion through the anolyte, operating as a natural electrolytic membrane. Indeed, the bacteria consortium growing on air breathing biocathodes consumes oxygen incoming from the cathode's porosity for their metabolism, actuating complex aerobic-anaerobic pathways [14]. In this way, they fit as an electrolytic barrier hampering the oxygen diffusion through the anode [15].

However, the biological ORR is usually the kinetic limiting step for single-chamber MFC processes. Furthermore, the biocathode suffers of carbonate deposits forming on the solid conductor beneath the biofilm, due to the local pH increase consequent to the ORR [16,17]. The exploration of highly performing ORR catalysts for cost-effective materials is therefore crucial to overcome these limitations.

Almost all conductive materials can support the growth of a thick biofilm and the mostly tested are carbon-based materials [1,10–18] and stainless steel [19,20]. ORR kinetics on cathodes takes place following different reaction mechanisms, depending on the material: i) through H_2O_2 intermediate formation ($2e^-$), ii) initial formation of H_2O_2 that is disproportionated into H_2O ($2x2e^-$), iii) directly forming H_2O transfer mechanism ($4e^-$) [21–23].

A micro-porous layer (MPL) based on carbon black or activated carbon (AC) is often used to increase the surface area for the bacteria settlement and to avoid corrosion [10,11,14–18]. AC is able to increase the ORR rate due to its high surface area, especially if enriched with carbon nanotubes [24,25], and thanks to catalytic functional groups [1,18]. Organic based catalysts (e.g. porphyrins [26] and phthalocyanines [27,28]) can be also added to improve AC performance.

Among Pt alternatives, other materials such as transition metals and metal oxides are excellent candidates, considering the positive feedback from the experience of other closely related

electrochemical technologies [1,27,29,30]. Nevertheless, they often express a relevant toxicity for bacteria as well for cells of living organisms.

In this context, the redox properties of CeO_2 nanoparticles have attracted the interest of the scientific community, being able to promote both oxygen evolution reaction (OER) and ORR [31]. Moreover, in biological systems $Ce^{4+/+3+}$ catalytically reacts with superoxide and hydrogen peroxide, mimicking superoxide dismutase (SOD) and catalase enzymatic activity [32–34], acting as antioxidant agent capable to abate all the reactive oxygen species (ROS)[35–38].

A previous work already demonstrated that the bioelectrochemical activity of bacteria was promoted by nanoceria at the anode of MFCs, improving the anode electron transfer efficiency and the power performance [39]. It has been reported that nanoceria could enhance the growth of some bacterial species while inhibiting others [40]. At the cathode, the capability of nanoceria to store and transfer oxygen on activated carbon was already tested in double chamber MFCs, but with a MnO_2 co-catalyst, in sterile conditions [41]. The results confirmed that nanoceria in synergy with MnO_2 was responsible of making oxygen available for a prolonged period enhancing the ORR rate and MFC performance, even if in a rather low performing system (~2403 mW/m^3).

Hence, the capability of nanoceria in enhancing the activity of air breathing carbon-based microbial cathodes in single-chamber MFCs was experimented in this work. CeO_2 and higher surface Sm doped nanoceria (Sm-CeO_2) nanoparticles were tested. The rationale was to decouple the effect of oxygen vacancies (oxygen storage ability) from that of the $Ce^{4+/3+}$ redox couples (direct electrocatalytic activity). In fact, Sm-CeO_2 nanoparticles, with 20% Sm, possess almost the same oxygen vacancy concentration than undoped nanoceria but with negligible Ce^{3+} ion concentration [37,38].

Microporous carbon cathode types were operated, in three different MFCs: i) a nanoceria added cathode MFC (CeO_2 MFC); ii) a samarium-doped ceria added cathode MFC (Sm-CeO_2 MFC); iii) a pristine carbon cathode MFC (Control MFC).

2. Materials and methods

2.1. Synthesis and characterization of CeO_2 and Sm-CeO_2 nanoparticles

The CeO_2 and 20 at% Sm-CeO_2 were produced with the same wet-chemical synthesis procedure reported in previous works, which also describe the characteristics not discussed here [31,36,42,43]. A post synthesis functionalization of 3-aminopropyltriethoxysilane dried nanoparticles was performed at pH 9.6 and 50 °C, starting from $Ce(NO_3)_3 \times 6H_2O$ and 6-{2-[2-(2-Methoxy-ethoxy)-ethoxy]-ethoxy}-hexyl)triethoxysilane.

The Brunauer-Emmett-Teller (BET) specific surface area was obtained from N_2 adsorption/desorption isotherms at 77 K using aMicromeritics Tristar II 3020 equipment. Before measurements, powder samples were heated to 150 °C for 4 h under a N_2 flow to remove adsorbed species. Measurements were performed more than three times to assess isotherms reproducibility and accuracy. Specific surface area values were determined using the instrument software. The porosity distribution was evaluated for each sample by using the Barrett-Joyner-Halenda (BJH) method applied to the N_2 adsorption data.

2.2. SEM analysis

The nanopowder morphology was characterized using scanning electron microscopy (SEM). Imaging was performed using a Leo 1430 SEM (Zeiss, Oberkochen, Germany).

Micrographs of biofilm on the operated CeO_2 cathode were also produced using a SEM Tescan Mira 3 – SEM field emission, at 20 KV. Cathode samples were cut, treated with glutaraldehyde 2%, dried with ethanol (20%, 40%, 60%, 80% and 95%), and finally coated with a carbon layer for SEM observations.

2.3. Electrodes

Anodes were made of carbon cloth (SAATI C1) without any surface treatment. 5 x 10 cm carbon cloth rectangles were cut and electrically connected to a plastic-insulated copper wire. A bi-component epoxy resin (PROCHIMA COLLA EPOXY) was used to insulate the electrical

connection. The electrical connection was tested for internal resistance and fluid contact/leakage by exposure to distilled water, as performed in previous tests [42].

Cathodes were fabricated by using 6 x 6 cm rectangles made of the same carbon cloth (SAATI C1) rectangles. The geometric surface area exposed to the wastewater was a circle with a 3 cm^2 area. The cathode was equipped with microporous layers that were prepared by mixing carbon black particles (TIMCAL ENSACO), polytetrafluoroethylene (PTFE) suspension, distilled water and a non-ionic surfactant (TritonTM X100, Sigma-Aldrich). Briefly, carbon black particles, distilled water and TritonTM X100 were added in a jar and mixed for 10 min. Then, a weighted amount of PTFE (60% dispersion in water, Sigma-Aldrich) was added to the solution and mixed for additional 10 min as to obtain a final PTFE percentage to carbon equal to 70 wt%. This slurry was spread and levelled onto carbon cloth rectangles and the excess was removed using a spatula. The resulting composite was then heated under static air for 30 min to 340 °C, aiming at evaporating water and decomposing the surfactant, near the PTFE melting point, as reported in a previous work [44]. The same procedure was repeated, layer by layer, three times on the same carbon cloth rectangle. The electrical connection to the external circuit was made directly connecting a copper wire to the carbon cloth and covering the connection with a thick layer of epoxy resin.

A suspension of either CeO_2 or Sm-CeO_2 samples dispersed in ethanol (11 mg mL^{-1}) was prepared, sonicated for 5 min, and drop-cast onto a cathode circular surface area of 3 cm^2. The final catalyst loading was calculated to be 1 mg cm^{-2}. Following the same procedure, three cathodes were prepared: i) pristine carbon cathodes as a control; ii) CeO_2-added cathodes; iii) Sm-CeO_2-added cathodes.

2.4. MFC setting

Single-chamber MFCs, without a polymeric membrane separating the anode from the cathode, were operated in batch mode at room temperature (25 ± 2 °C). Electrodes (anode and cathode projected areas of 100 cm^2 and 3 cm^2, respectively) were positioned at a relative distance of 2 cm. A Pyrex bottle of 125 mL was equipped with a large Pyrex flange on one side, to settle the open-air cathode,

as illustrated in Figure S1 of Supplementary information. The catalyst layer was exposed to the wastewater side and the anode was positioned inside the bottle. The bottle top was sealed with a hermetic plastic screw cap.

The tests were performed using as medium and inoculum swine manure, sampled in a pig-farm near Milan (Italy). Concentrated swine manure (COD = 13 g L^{-1}) was diluted (1:10) with a carbonate buffer (pH 7.8, 0.1 M) to avoid organic/inorganic overloads.

After inoculation, the anode and the cathode were connected to a 100 Ω external load. Cell potential difference was recorded every 20 min across the load using a multichannel data logger (Graphtec midi LOGGER GL820). The generated current (I) was calculated using the Ohm's law ($I = V R^{-1}$, where R is the external resistive load and V is the cell potential difference) and normalized by the cathode area to obtain the current density (j). After the current generation dropped, sodium acetate (Aldrich) was added to the anodic chamber (0.036 mol L^{-1} concentration) as a fuel for bacterial metabolism in subsequent batch cycles.

The anolyte conductivity varied from 2 ± 0.1 mS/cm at the beginning of the fed cycle to 1.2 ± .3 mS/cm at the end of the cycle.

2.6. Electrochemical characterization

Nanopowders

Preliminary electrochemical characterization of the two CeO_2-based nanopowders was performed in phosphate buffer solution (pH 7.8) and 0.1 mol L^{-1} KOH (pH 14) using cyclic voltammetry (CV) through a potentiostat (Amel mod. 7050). Catalyst aliquots were dispersed in ethanol, sonicated for 5 min and pipetted onto the glassy carbon tip (geometric surface area: A = 0.07 cm^2, EDI 101, Radiometer) and dried in a bottom-up position over a tungsten lamp (100 W). Ceria-based electrocatalyst loading was 1 mg cm^{-2}. A two-compartment cell with a graphite counter electrode (Amel 201/S-016) and an Ag/AgCl external reference electrode (Amel) in 3 mol L^{-1} NaCl was used. Before the recording of CV curves, the working electrode was conditioned by cycling 45 min in N_2 saturated 0.1 mol L^{-1} KOH within the E = −0.900 / +0.150 V potential range. When using carbonate buffer solution, the potential range was E = −1.2 / +0.1 V. This step was followed by 100 min

cycling in O_2 saturated solution (v = 0.005 V s^{-1}). CV curves in O_2 were recorded at the same conditions. After measurements in O_2, CV curves were again recorded in N_2 to obtain background faradaic currents for O_2 reduction data correction.

MFC system

The anodic and cathodic open-circuit potential (OCP) values for each MFC system were periodically measured *vs* an Ag/AgCl (KCl sat.; 0.198 vs SHE) reference electrode, after 2 h equilibration time. Cell OCP values were also measured.

Power curves were periodically recorded with a two-electrode configuration. Before each electrochemical measurement, 2 h equilibration time was found necessary to allow the MFC system, disconnected from the data logger, to reach its OCP. The anode was set as working electrode and the cathode as reference electrode. A linear sweep polarization (v = 0.010 V min^{-1}) was recorded from the cell OCP to 10 mV. Power (P) was calculated by $P = I \times V$ and plotted against the current density (j) referred to the geometric area of the cathode (3 cm^2).

Coulumbic efficiency (CE) was calculated by comparing the actual electric charge produced during each feed cycle to the available charge of the dosage (0.036 mol L^{-1} acetate) supposing that all the acetate was consumed during the cycle.

Polarization curves on the cathodes were also periodically performed, using a three-electrode configuration with a graphite rod as a counter electrode, and an Ag/AgCl in KCl (sat.) as reference electrode. Before each measurements, the working cell was left at open circuit potential (OCP) for at least 1 h and then the analysis was performed. The scan rate was v = 0.010 V min^{-1}.

3. Results and Discussion

3.1. CeO_2 and Sm-CeO_2 preliminary characterization

SEM analysis was initially used to investigate the catalyst morphology and dispersion onto the carbon-based cathodic surfaces. Figure 1 shows the micrographs of the carbon-based cathodes added with CeO_2 nanoparticles (Figs. 1A, 1C) and added with Sm-CeO_2 nanoparticles (Figs. 1B, 1D). Figures 1A and 1B show the formation of a uniform particle film on the carbon, interrupted by few

cracks, with the presence of nearly spherical large particles of micrometric size. The aggregates were more pronounced for the Sm-CeO_2, as shown in Fig. 1B. The micrographs at higher magnification (Fig. 1C and 1D) showed that the particles preserved their nanostructure, even though the Sm-CeO_2 particles displayed a smaller average size (several nm).

In agreement with the SEM observations, the N_2 adsorption/desorption isotherms (Fig. 2A) showed that the BET specific surface area (SSA) values for CeO_2 and Sm-CeO_2 were 51 ± 3 m^2 g^{-1} and 145 ± 7 m^2 g^{-1}, respectively.

Contrary to what previously reported [37], a three-fold increase in SSA was observed upon Sm introduction and solid solution formation during the synthesis. However, Li *et al.* [45] observed that doping cerium oxide with 20 at% samarium increased the lattice parameter of the parent structure and effectively inhibited crystallite growth during nanoparticle synthesis, resulting in smaller particle size and larger surface area. The pore area distribution in the 2-125 nm range (Fig. 2B) showed the shift of the maximum peak for Sm-CeO_2 particles to 20 nm from 40 nm for CeO_2 particles, thus confirming the more pronounced nanostructured nature of the Sm-CeO_2 [45].

Both samples are characterized by an isotherm of Type IV. In fact, their hysteresis loop is associated with capillary condensation taking place in mesopores and the limiting uptake lies over a range of high p/p°, more visible in Sm-CeO_2 isotherm. The initial part of the Type IV isotherm is attributed to monolayer-multilayer adsorption. The corresponding hysteresis loop is ascribable to Type H1, attributable to porous materials constituted by agglomerates or compacts of approximately uniform spheres in fairly regular array [46].

The electrocatalytic properties towards ORR of CeO_2 and Sm-CeO_2 deposited on a glassy carbon (GC) was investigated by polarization curves. The deposition of the nanocatalysts on conducting substrates such as GC is an efficient strategy adopted to increase their conductivity [47]. Figure 3A shows the cathodic polarization curves for ORR recorded in carbonate buffer solution (pH 7.8) for the three samples with the current density being normalized by the GC electrode area (0.07 cm^2). As expected, the bare GC electrode displayed poor catalytic behaviour for ORR: the limiting current was undetectable and the onset potential (E_{on}) calculated by the tangent method (about -0.350 V vs.

SHE) is 0.650 V lower than the E_{on} observed for a commercial Pt catalyst (0.5 mg cm^{-2}) in similar pH condition (E_{on} = 0.3 V vs. SHE) [20].

The GC electrodes covered by CeO_2 and Sm-CeO_2 showed a higher E_{on} for ORR than bare GC (black-solid and black-dotted lines in Fig. 3A): -0.150 V (vs. SHE) and +0.050 V (vs. SHE) measured for the CeO_2 and Sm-CeO_2 samples, respectively.

These results confirm that ceria plays an important contribution to the ORR activity, definitely improved with respect to the GC, although without reaching the state-of-the-art ORR electrocatalyst performance [21]. Indeed, a limiting current density was detectable (about 1.4 10^{-4} A cm^{-2}). It is well known that the defects induced by oxygen vacancies dominate the electronic and chemical properties of CeO_2. The increase in oxygen vacancy concentration can reduce the band gap and elongate the O-O bond of the adsorbed O_2, enhancing the catalytic ability of CeO_2 for ORR [48].

The superior catalytic properties displayed by the Sm-doped nanoceria can be justified by the presence of the smallest grains whit highest specific surface area [48,49].

From the chemical point of view, proton reaction in ORR and the formation of OH^- as final product causes the local alkalinization of the cathode. Several works demonstrated that an electrocatalysis improvement is usually expected at alkaline pH [50–52]. This is due to the improved stability at high pH of intermediate hydroperoxide anions that enable a complete $4e^-$ transfer on the active sites [51]. High pH, up to 12-13, was measured near the cathode also in operating single-chamber MFCs [11]. Taking into account these aspects, the cathodic polarization curves were repeated in 0.1 mol L^{-1} KOH solution (Fig. 3B). The results confirmed that the ORR onset potential at pH 13 were shifted to less cathodic values, as expected, for bare GC and CeO_2 catalyst (by 0.150 V than in the carbonate buffer). Nevertheless, the ORR onset potential of Sm-CeO_2 catalyst maintained the same value (0.050 V vs. SHE) at alkaline pH, as well as in the neutral buffer. This is explained by a different oxygen binding strength in the two catalysts. Catalysts based on a redox system as $Ce^{4+/3+}$, with weak O_2 binding (i.e. positive redox potential) reduce oxygen at an onset potential that shifts towards more positive values in the SHE scale by a pH increase; on the other hand, catalysts based on a redox system characterized by a strong O_2 binding, such as Sm (i.e. negative redox potential), reduce oxygen at an onset potential that is independent from the pH [53].

3.2. MFC electrochemical behaviour

Figure 4A shows the current trend achieved operating the MFCs with different cathodes and measured through the resistance of 100 Ω, during five cycle of acetate (0.036 mol L^{-1}) dosage.Sm-CeO_2 MFC was always the best performing cell throughout the 75 days operation.

The generated power values of 113 mWh m^{-2} and 65 mWh m^{-2} were estimated from the current trends, produced by Sm-CeO_2 and CeO_2 MFCs, respectively.

Only 31 mWh m^{-2} was produced by control MFC. Therefore, Ce-based cathodes significantly improved performance, despite the intrinsic limitations in the MFC set-up, due for instance to the high PTFE content used in the cathode [44].

During the feed cycle 1, the current density in Sm-CeO_2 MFC reached 1867 mA m^{-2}, much larger than the peak of 1290 mA m^{-2} reached in the CeO_2 MFC. During feed cycle 2, the Sm-CeO_2 MFC reached again higher current value (2100 mA m^{-2}) than the CeO_2 MFC (1680 mA m^{-2}). The gap between the current peaks narrowed over time and current densities overlapped at almost 2500-2750 mA m^{-2} during feed cycle 3 and 4. Nevertheless, the Sm-CeO_2 MFC remained the best performing sample, being characterized by longer lasting acetate feed cycle.

Each MFC type had slightly better performance cycle by cycle, during the whole test (Fig. 4A). The current density increase might be assigned to the formation over time of an electroactive biofilm, especially thick on the cathode (Figure S2 and S3). The proof of an enhancement of the bacteria activity on electrodes can be also inferred by the increase of the coulombic efficiency (Table 1). This phenomenon did not depend upon the anode and cathode OCPs, which fluctuated and then finally stabilized at similar values, as evidenced from Fig. 4C and 4D.

The anode OCPs were similar for the three MFCs, with a tendency to be lower than the others for the Sm-CeO_2 MFC (Fig. 4C). In this last case, the higher values of the cathode OCP during the first two cycles (0.1 V more positive than the others; Fig. 4D), did not correspond to the higher performance of this cathode, confirming that the Sm-CeO_2 MFC cathodic reaction mostly benefited by the synergistic presence of the chemical catalyst and the growth of an electroactive biofilm.

The carbonate buffer was able to control the pH in a range favourable for the microorganism growth during all the 70 days experimentation, as neither significant alkalization, nor acidification of the solution occurred (Fig. 4C). pH in the bulk of anolyte slightly varied during remaining cycles between 7-9, a safe range for the bacteria life [54,55], although a more pronounced variation could have more likely occurred near the electrodes beneath the biofilms, as previously documented [15,54].

From day 63, the fast and definitive decline in performance for all the MFCs (few days earlier for CeO_2 MFC) was likely due to alkalinization and the precipitation over time of a carbonate wall beneath the cathodic biofilm, as previously documented for this type of cathodes and carbonate buffered media [16]. In the end, the abundance of carbonates in the buffered solution strongly limited the cathode.

Indeed, after the fifth cycle, the acetate addition to MFCs (day 70) was no longer successful in producing current, and the test was interrupted.

The image of the operated cathodes, enriched in carbonate, is reported in Figure S2- S5. Dried deposits on the CeO_2 cathode found under the biofilm is reported in Figure S4. The carbonate deposit resistant to mechanical and hydraulic cleaning of the Sm-CeO_2 cathode is shown in Figure S5.

Figure 5 shows the SEM micrographs of the operated CeO_2 cathode, collected in different areas of the samples. Bacteria on the external surface of the biofilm are clearly visible in Figure 5A. In Figure 5B details of colonized CeO_2 nanoparticles are underlined (EDS element analysis in Figure 5D); Figure 5C shows carbonates particles growing in the cathode under the biofilm (EDS element analysis in Figure 5E).

Figure 6A shows the cathode polarization curves recorded at day t = 0 and under feeding conditions in representative cycle 1 and 3. At t = 0 and during cycle 1, the Sm-CeO_2 cathode displayed higher current densities than CeO_2 cathode and control cathode, the latter characterized by very low current density.

The improved performance of each cathode is still in agreement with the growth and stabilization of a catalytic active biofilm under feeding conditions. Only later, at cycle 3, the CeO_2 biocathode reached a current production similar to that of Sm-CeO_2 one. The early higher performance of the

Sm-CeO_2 cathode might be associated to a local increase of pH under the biofilm, at more favourable values for the CeO_2 ORR catalyst, which did not produce an equivalent high performance in terms of MFC generated current density (Fig. 6A) and power density (Fig 6B). This is likely ascribable to a not still mature anodic biofilm at that time. Figure 6B shows the power curves recorded at acclimation and feeding cycles 1 and 3. During the initial acclimation, all the recorded power curves were characterized by a relatively low maximum power density (P_{max}) ranging between 0.04 and 0.06 W m^{-2}. During cycle 1, the power peak of the control MFC reached a slightly higher value compared to the acclimation period, similar to the CeO_2 MFC and Sm-CeO_2 MFC which were characterized by P_{max} of 0.13 W m^{-2} and 0.18 W m^{-2}, respectively. The peak power density values of the CeO_2 MFC and Sm-CeO_2 MFC were further enhanced from the cycle 1 to cycle 3 up to similar values (P_{max} = 0.21 W m^{-2} and 0.22 W m^{-2}, respectively). From day 40 onward, indeed, Sm-CeO_2 MFC and CeO_2 MFC performed similarly. Based on these results, it could be hypothesized that the growing carbonate scale introduced a physical obstacle under the biofilm [16], causing a coulombic efficiency decay of CeO_2 MFC in the last cycle and nullifying the advantage of the higher initial surface area of the Sm-CeO_2 nanopowder.

3.4. Nanoceria oxygen storage ability

Many of the applications of ceria nanoparticles arise from the low redox potential between the Ce^{3+} and Ce^{4+} oxidation states and the high mobility of oxygen vacancies in the nanosize regime [56]. Oxygen vacancies are created to guarantee charge neutrality. Due to this phenomenon, which increases oxygen diffusion, ceria can easily absorb and release oxygen being a well-known oxygen-storage material [31]. The lattice constant and Ce^{3+} concentration are increased with decreasing the particle size [57], since the concentration of defects is larger at the subsurface layer [58]. The substitution of trivalent elements, such as Sm, in the Ce lattice sites can also enhance the formation of oxygen vacancies. Two Ce^{4+} ions are replaced by two trivalent cations in the ceria lattice [56]. Therefore, in the Sm-doped ceria the concentration of oxygen vacancies is almost the same as in the undoped ceria, but the Ce^{3+} concentration is reduced, hindering the possibility to exploit the $Ce^{4+/3+}$ redox couple [37].

This is important for understanding the improved ORR mechanism, since it may be caused either by increased oxygen storage ability, due to oxygen vacancies, or by a direct increase in the electrocatalytic activity through the $Ce^{4+/3+}$ redox couples. In fact, Peng *et al.* [47] demonstrated that CeO_2 was able to enhance the ORR electroactivity of carbon-based systems such as graphene with a direct enhancement of the oxygen reduction reaction. It is also known that oxygen-defect formation is accompanied by localization of the electrons left behind in Ce 4f states, leading to formation of two Ce^{3+} ions [59]. The oxygen vacancy concentration increase reduces the band gap and elongates the O-O bond of the adsorbed O_2. The catalytic activity of CeO_2 for ORR is consequently enhanced. In addition, the valence switch between Ce^{3+} and Ce^{4+} gives to cerium oxide redox ability; Ce^{4+} ions and the surface vacancies play a significant role for oxidation, while the Ce^{3+} ions and electron shuffling within the lattice oxygen vacancies are important for reduction [59]. Hence, an ORR electrocatalytic activity enhancement might be related to oxygen-defects in cerium oxide nanoparticles acting as active oxygen adsorption sites, and/or Ce^{3+} and electron shuffling within the lattice oxygen vacancies, improving the catalysis of the oxygen reduction.

These two aspects, ceria oxygen storage ability and ceria electrocatalytic activity, are both crucial in the explanation of the enhanced performance of Sm-CeO_2 MFC and CeO_2 cathode MFC with respect to the control cathode MFC. The microporous layer on which ceria-based nanopowders were deposited in the case of Sm-CeO_2 MFC and CeO_2 MFC is subjected to anaerobic conditions, being exposed to the anolyte side and colonized of anaerobic or microaerophilic bacteria for a large extent [11,14]. Hence, without any additional help, the final cathodic reactant - oxygen - is impeded by diffusion resistance in reaching the catalytic sites, as well as the mediators produced by bacteria. However, due to the presence of ceria-based nanoparticles that act as an oxygen reservoir, the reactant lack at the interface between electrodes and biofilm is lowered. The fact that both Sm-doped and undoped ceria nanoparticles work similarly and better when the biofilm is developed, demonstrates that this is the main mechanism for ORR catalysis enhancement. The larger specific surface area of Sm-CeO_2 sample can explain the further enhancement in ORR electrocatalysis. The differences in current production between Sm-CeO_2 MFC and CeO_2 MFC found within the first 40 days operation (Fig. 3) might be ascribed to the Sm favoured ORR at pH around 8, other than to the

higher specific active surface. After day 40, a local growth of $CaCO_3$ deposits beneath cathodic biofilm might have affected these conditions. In fact, the MFCs with CeO_2 and Sm-CeO_2 cathodes started producing the same current, although acetate cycles were longer lasting in Sm-CeO_2 system, which reached in this way the highest coulombic efficiency (Table 1). This is correlated with a bioanode performance improvement, which deserves further investigation. Notably, it can be concluded that the role played by the Ce redox couple on ORR is minor in the presence of a biofilm on the cathode.

The good affinity of nanoceria with the electroactive system of a microbial fuel cell in long lasting tests suggests that the bacteria pool does not suffer, but rather takes advantage of its presence, as Figures 5 and S3 report colonized nanoceria particles. This is an important result since it suggests that nanoceria can be considered a promising candidate for electrochemical applications where the biocompatibility with the microbial pool is a relevant issue [57].

Conclusions

Nanoceria in air breathing carbon biocathodes enables more than a two-fold increase of the electric energy generated in single-chamber MFCs. Sm-doped CeO_2 nanoparticles with high specific surface area maximize the performance of the microbial cathodes studied in the present work, settling their central role as oxygen reservoir for cathodic biofilm. Nano-CeO_2 particles stimulate the microbial biocathode electroactivity having consequently a beneficial effect on the electroactive performance of the bioanode, during successive feeding cycles. Future effort will be addressed in optimizing the carbon structure of the cathodes and their porosity, as well as on the studies of the specific influence on the anode activity in a perspective of powerful and long lasting bioelectrochemical application.

Conflicts of interest

There are no conflicts to declare.

Acknowledgements

This work has been financed by the Research Fund for the Italian Electrical System in compliance with the Decree of Minister of Economic Development April 16, 2018.

References

[1] C. Santoro, C. Arbizzani, B. Erable, I. Ieropoulos, Microbial fuel cells: From fundamentals to applications. A review, J. Power Sources. 356 (2017) 225–244. doi:10.1016/J.JPOWSOUR.2017.03.109.

[2] W.-W. Li, H.-Q. Yu, Z. He, H. Yu, Y. Raichlin, A. Katzir, B. Mizaikoff, K. Kubota, Y.Y. Li, H. Harada, H.Q. Yu, A. Schramm, N. Risgaard-Petersen, L.P. Nielsen, J.N. Butt, D.J. Richardson, Towards sustainable wastewater treatment by using microbial fuel cells-centered technologies, Energy Environ. Sci. 7 (2013) 911–924. doi:10.1039/C3EE43106A.

[3] Y. Fan, S.-K. Han, H. Liu, Improved performance of CEA microbial fuel cells with increased reactor size, Energy Environ. Sci. 5 (2012) 8273. doi:10.1039/c2ee21964f.

[4] P. Roustazadeh Sheikhyousefi, M. Nasr Esfahany, A. Colombo, A. Franzetti, S.P. Trasatti, P. Cristiani, Investigation of different configurations of microbial fuel cells for the treatment of oilfield produced water, Appl. Energy. (2016). doi:10.1016/j.apenergy.2016.10.057.

[5] K. Raman, J.C.W. Lan, Performance and kinetic study of photo microbial fuel cells (PMFCs) with different electrode distances, Appl. Energy. 100 (2012) 100–105. doi:10.1016/j.apenergy.2012.03.011.

[6] A. Rinaldi, B. Mecheri, V. Garavaglia, S. Licoccia, P. Di Nardo, E. Traversa, Engineering materials and biology to boost performance of microbial fuel cells: a critical review, Energy Environ. Sci. 1 (2008) 417. doi:10.1039/b806498a.

[7] W.W. Li, H.Q. Yu, Stimulating sediment bioremediation with benthic microbial fuel cells, Biotechnol. Adv. 33 (2015) 1–12. doi:10.1016/j.biotechadv.2014.12.011.

[8] I.A. Ieropoulos, J. Greenman, C. Melhuish, I. Horsfield, Microbial Fuel Cells for Robotics: Energy Autonomy through Artificial Symbiosis, ChemSusChem. 5 (2012) 1020–1026. doi:10.1002/cssc.201200283.

[9] D.N. Roxby, N. Tran, P.-L. Yu, H.T. Nguyen, Experimenting with microbial fuel cells for powering implanted biomedical devices, in: 2015 37th Annu. Int. Conf. IEEE Eng. Med. Biol. Soc., IEEE, 2015: pp. 2685–2688. doi:10.1109/EMBC.2015.7318945.

[10] C. Santoro, Y. Lei, B. Li, P. Cristiani, Power generation from wastewater using single chamber microbial fuel cells (MFCs) with platinum-free cathodes and pre-colonized anodes, Biochem. Eng. J. 62 (2012) 8–16. doi:10.1016/j.bej.2011.12.006.

[11] P. Cristiani, M.L. Carvalho, E. Guerrini, M. Daghio, C. Santoro, B. Li, Cathodic and anodic biofilms in Single Chamber Microbial Fuel Cells., Bioelectrochemistry. 92 (2013) 6–13. doi:10.1016/j.bioelechem.2013.01.005.

[12] C. Santoro, S. Babanova, P. Atanassov, B. Li, I. Ieropoulos, P. Cristiani, High Power Generation by a Membraneless Single Chamber Microbial Fuel Cell (SCMFC) Using Enzymatic Bilirubin Oxidase (BOx) Air-Breathing Cathode, J. Electrochem. Soc. 160 (2013) H720–H726. doi:10.1149/2.058310jes.

[13] S. Chen, S.A. Patil, U. Schröder, A high-performance rotating graphite fiber brush air-cathode for microbial fuel cells, Appl. Energy. 211 (2018) 1089–1094. doi:10.1016/j.apenergy.2017.12.013.

[14] L. Rago, P. Cristiani, F. Villa, S. Zecchin, A. Colombo, L. Cavalca, A. Schievano, Influences of dissolved oxygen concentration on biocathodic microbial communities in microbial fuel cells, Bioelectrochemistry. 116 (2017). doi:10.1016/j.bioelechem.2017.04.001.

[15] E. Guerrini, M. Grattieri, S.P. Trasatti, M. Bestetti, P. Cristiani, Performance explorations of single chamber microbial fuel cells by using various microelectrodes applied to biocathodes, Int. J. Hydrogen Energy. 39 (2014) 21837–21846. doi:10.1016/j.ijhydene.2014.06.132.

[16] M. Santini, S. Marzorati, S. Fest-Santini, S. Trasatti, P. Cristiani, Carbonate scale deactivating the biocathode in a microbial fuel cell, J. Power Sources. 356 (2017) 400–407. doi:10.1016/j.jpowsour.2017.02.088.

[17] M. Santini, M. Guilizzoni, M. Lorenzi, P. Atanassov, E. Marsili, S. Fest-Santini, P. Cristiani, C. Santoro, Three-dimensional X-ray microcomputed tomography of carbonates and biofilm on operated cathode in single chamber microbial fuel cell, Biointerphases. 10 (2015) 031009. doi:10.1116/1.4930239.

[18] C. Santoro, K. Artyushkova, S. Babanova, P. Atanassov, I. Ieropoulos, M. Grattieri, P. Cristiani, S. Trasatti, B. Li, A.J. Schuler, Parameters characterization and optimization of activated carbon (AC) cathodes for microbial fuel cell application, Bioresour. Technol. 163 (2014) 54–63. doi:10.1016/j.biortech.2014.03.091.

[19] E. Guerrini, P. Cristiani, M. Grattieri, C. Santoro, B. Li, S. Trasatti, Electrochemical Behavior of Stainless Steel Anodes in Membraneless Microbial Fuel Cells, J. Electrochem. Soc. 161 (2014) H62–H67. doi:10.1149/2.096401jes.

[20] D. Pocaznoi, A. Calmet, L. Etcheverry, B. Erable, A. Bergel, Stainless steel is a promising electrode material for anodes of microbial fuel cells, Energy Environ. Sci. 5 (2012) 9645. doi:10.1039/c2ee22429a.

[21] M.T. Nguyen, B. Mecheri, A. Iannaci, A. D'Epifanio, S. Licoccia, Iron/Polyindole-based Electrocatalysts to Enhance Oxygen Reduction in Microbial Fuel Cells, Electrochim. Acta. 190 (2016) 388–395. doi:10.1016/j.electacta.2015.12.105.

[22] C. Santoro, M. Kodali, S. Kabir, F. Soavi, A. Serov, P. Atanassov, Three-dimensional graphene nanosheets as cathode catalysts in standard and supercapacitive microbial fuel cell, J. Power Sources. 356 (2017) 371–380. doi:10.1016/J.JPOWSOUR.2017.03.135.

[23] W. Yang, B.E. Logan, Immobilization of a Metal-Nitrogen-Carbon Catalyst on Activated Carbon with Enhanced Cathode Performance in Microbial Fuel Cells, ChemSusChem. 9 (2016) 2226–2232. doi:10.1002/cssc.201600573.

[24] Z. Chen, M. Waje, W. Li, Y. Yan, Supportless Pt and PtPd Nanotubes as Electrocatalysts for Oxygen-Reduction Reactions, Angew. Chemie Int. Ed. 46 (2007) 4060–4063. doi:10.1002/anie.200700894.

[25] R. Bresciani, S. Marzorati, A. Lascialfari, B. Sacchi, N. Santo, M. Longhi, Effects of catalyst aging on the growth morphology and oxygen reduction activity of nitrogen-doped carbon nanotubes, Electrochem. Commun. 51 (2015) 27–32. doi:10.1016/j.elecom.2014.12.003.

[26] S. Kim, H. Kim, Oxygen reduction reaction at porphyrin-based electrochemical catalysts: Mechanistic effects of pH and spin states studied by density functional theory, Catal. Today. 295 (2017) 119–124. doi:10.1016/J.CATTOD.2017.05.007.

[27] C. Santoro, R. Gokhale, B. Mecheri, A. D'Epifanio, S. Licoccia, A. Serov, K. Artyushkova, P. Atanassov, Design of Iron(II) Phthalocyanine-Derived Oxygen Reduction Electrocatalysts for High-Power-Density Microbial Fuel Cells, ChemSusChem. 10 (2017) 3243–3251. doi:10.1002/cssc.201700851.

[28] R. Chen, H. Li, D. Chu, G. Wang, Unraveling Oxygen Reduction Reaction Mechanisms on Carbon-

Supported Fe-Phthalocyanine and Co-Phthalocyanine Catalysts in Alkaline Solutions, J. Phys. Chem. C. 113 (2009) 20689–20697. doi:10.1021/jp906408y.

[29] M. Kodali, C. Santoro, A. Serov, S. Kabir, K. Artyushkova, I. Matanovic, P. Atanassov, Air Breathing Cathodes for Microbial Fuel Cell using Mn-, Fe-, Co- and Ni-containing Platinum Group Metal-free Catalysts, Electrochim. Acta. 231 (2017) 115–124. doi:10.1016/J.ELECTACTA.2017.02.033.

[30] C. Santoro, A. Serov, R. Gokhale, S. Rojas-Carbonell, L. Stariha, J. Gordon, K. Artyushkova, P. Atanassov, A family of Fe-N-C oxygen reduction electrocatalysts for microbial fuel cell (MFC) application: Relationships between surface chemistry and performances, Appl. Catal. B Environ. 205 (2017) 24–33. doi:10.1016/j.apcatb.2016.12.013.

[31] V. Esposito, E. Traversa, Design of Electroceramics for Solid Oxides Fuel Cell Applications: Playing with Ceria, J. Am. Ceram. Soc. 91 (2008) 1037–1051. doi:10.1111/j.1551-2916.2008.02347.x.

[32] C. Korsvik, S. Patil, S. Seal, W.T. Self, Superoxide dismutase mimetic properties exhibited by vacancy engineered ceria nanoparticles, Chem. Commun. (2007) 1056. doi:10.1039/b615134e.

[33] C. Walkey, S. Das, S. Seal, J. Erlichman, K. Heckman, L. Ghibelli, E. Traversa, J.F. McGinnis, W.T. Self, E.C. Lavelle, L.A. O'Neill, J.G. Hollyfield, P. Humphries, E.A. Grulke, P. Di Nardo, T. Hyeon, R.K. Hailstone, J.S. Erlichman, Catalytic properties and biomedical applications of cerium oxide nanoparticles, Environ. Sci. Nano. 2 (2015) 33–53. doi:10.1039/C4EN00138A.

[34] T. Pirmohamed, J.M. Dowding, S. Singh, B. Wasserman, E. Heckert, A.S. Karakoti, J.E.S. King, S. Seal, W.T. Self, Nanoceria exhibit redox state-dependent catalase mimetic activity., Chem. Commun. 46 (2010) 2736–8. doi:10.1039/b922024k.

[35] I. Celardo, J.Z. Pedersen, E. Traversa, L. Ghibelli, Pharmacological potential of cerium oxide nanoparticles, Nanoscale. 3 (2011) 1411. doi:10.1039/c0nr00875c.

[36] F. Pagliari, C. Mandoli, G. Forte, E. Magnani, S. Pagliari, G. Nardone, S. Licoccia, M. Minieri, P. Di Nardo, E. Traversa, Cerium Oxide Nanoparticles Protect Cardiac Progenitor Cells from Oxidative Stress, ACS Nano. 6 (2012) 3767–3775. doi:10.1021/nn2048069.

[37] I. Celardo, M. De Nicola, C. Mandoli, J.Z. Pedersen, E. Traversa, L. Ghibelli, Ce 3+ Ions Determine Redox-Dependent Anti-apoptotic Effect of Cerium Oxide Nanoparticles, ACS Nano. 5 (2011) 4537–4549. doi:10.1021/nn200126a.

[38] F. Caputo, M. De Nicola, A. Sienkiewicz, A. Giovanetti, I. Bejarano, S. Licoccia, E. Traversa, L. Ghibelli, Cerium oxide nanoparticles, combining antioxidant and UV shielding properties, prevent UV-induced cell damage and mutagenesis., Nanoscale. 7 (2015) 15643–56. doi:10.1039/c5nr03767k.

[39] Y. Yin, G. Huang, N. Zhou, Y. Liu, L. Zhang, Increasing power generation of microbial fuel cells with a nano-CeO_2 modified anode, Energy Sources, Part A Recover. Util. Environ. Eff. 38 (2016) 1212–1218. doi:10.1080/15567036.2014.898112.

[40] I. Kamika, M. Tekere, Impacts of cerium oxide nanoparticles on bacterial community in activated sludge., AMB Express. 7 (2017) 63. doi:10.1186/s13568-017-0365-6.

[41] I. Singh, A. Chandra, Use of the oxygen storage material CeO2 as co-catalyst to improve the performance of microbial fuel cells, Int. J. Hydrogen Energy. 41 (2015) 1913–1920. doi:10.1016/j.ijhydene.2015.10.130.

[42] F. Caputo, M. Mameli, A. Sienkiewicz, S. Licoccia, F. Stellacci, L. Ghibelli, E. Traversa, A novel synthetic approach of cerium oxide nanoparticles with improved biomedical activity, Sci. Rep. 7 (2017) 4636. doi:10.1038/s41598-017-04098-6.

[43] C. Mandoli, F. Pagliari, S. Pagliari, G. Forte, P. Di Nardo, S. Licoccia, E. Traversa, Stem Cell

Aligned Growth Induced by CeO2 Nanoparticles in PLGA Scaffolds with Improved Bioactivity for Regenerative Medicine, Adv. Funct. Mater. 20 (2010) 1617–1624. doi:10.1002/adfm.200902363.

[44] E. Guerrini, M. Grattieri, A. Faggianelli, P. Cristiani, S. Trasatti, PTFE effect on the electrocatalysis of the oxygen reduction reaction in membraneless microbial fuel cells, Bioelectrochemistry. 106 (2015) 240–247. doi:10.1016/j.bioelechem.2015.05.008.

[45] J.-G. Li, Y. Wang, T. Ikegami, T. Mori, T. Ishigaki, Reactive 10mol% RE2O3 (RE=Gd and Sm) doped CeO2 nanopowders: Synthesis, characterization, and low-temperature sintering into dense ceramics, Mater. Sci. Eng. B. 121 (2005) 54–59. doi:10.1016/j.mseb.2005.03.001.

[46] K.S.W. Sing, D.H. Everett, R.A.W. Haul, L. Moscou, R.A. Pierotti, J. Rouquerol, T. Siemieniewska, K.S.W. Sing, D.H. Everett, R.A.W. Haul, L. Moscou, R.A. Pierotti, J. Rouquerol, T. Siemieniewska, Reporting Physisorption Data for Gas/Solid Systems, in: Handb. Heterog. Catal., Wiley-VCH Verlag GmbH & Co. KGaA, Weinheim, Germany, 2008. doi:10.1002/9783527610044.hetcat0065.

[47] W. Peng, L. Zhao, C. Zhang, Y. Yan, Y. Xian, Controlled growth cerium oxide nanoparticles on reduced graphene oxide for oxygen catalytic reduction, Electrochim. Acta. 191 (2016) 669–676. doi:10.1016/j.electacta.2016.01.129.

[48] X. Yuan, H. Ge, X. Liu, X. Wang, W. Chen, W. Dong, F. Huang, Efficient catalyst of defective CeO2−x and few-layer carbon hybrid for oxygen reduction reaction, J. Alloys Compd. 688 (2016) 613–618. doi:10.1016/j.jallcom.2016.07.060.

[49] J. Bae, S. Hong, B. Koo, J. An, F.B. Prinz, Y.-B. Kim, Influence of the grain size of samaria-doped ceria cathodic interlayer for enhanced surface oxygen kinetics of low-temperature solid oxide fuel cell, J. Eur. Ceram. Soc. 34 (2014) 3763–3768. doi:10.1016/j.jeurceramsoc.2014.05.028.

[50] M. Kodali, C. Santoro, S. Herrera, A. Serov, P. Atanassov, Bimetallic platinum group metal-free catalysts for high power generating microbial fuel cells, J. Power Sources. 366 (2017) 18–26. doi:10.1016/j.jpowsour.2017.08.110.

[51] N. Ramaswamy, S. Mukerjee, N. Ramaswamy, S. Mukerjee, Fundamental Mechanistic Understanding of Electrocatalysis of Oxygen Reduction on Pt and Non-Pt Surfaces: Acid versus Alkaline Media, Adv. Phys. Chem. 2012 (2012) 1–17. doi:10.1155/2012/491604.

[52] Z. He, Y. Huang, A.K. Manohar, F. Mansfeld, Effect of electrolyte pH on the rate of the anodic and cathodic reactions in an air-cathode microbial fuel cell, Bioelectrochemistry. 74 (2008) 78–82. doi:10.1016/j.bioelechem.2008.07.007.

[53] K. Uosaki, Electrochemical science for a sustainable society : a tribute to John O'M Bockris, Springer, n.d. https://books.google.it/books?id=C3koDwAAQBAJ&pg=PA39&lpg=PA39&dq=%22weak+o2+binding%22+%22positive+redox+potential%22&source=bl&ots=z7qPTOewJC&sig=ACfU3U0MyW-BlBjBoCc8J13TfyleP9azlw&hl=it&sa=X&ved=2ahUKEwjhy9mEntngAhUKzqQKHek3Dd0Q6AEwAHoECAAQAQ#v=onepage (accessed February 26, 2019).

[54] M. Rahimnejad, A. Adhami, S. Darvari, A. Zirepour, S.-E. Oh, Microbial fuel cell as new technology for bioelectricity generation: A review, Alexandria Eng. J. 54 (2015) 745–756. doi:10.1016/j.aej.2015.03.031.

[55] D. Jiang, M. Curtis, E. Troop, K. Scheible, J. McGrath, B. Hu, S. Suib, D. Raymond, B. Li, A pilot-scale study on utilizing multi-anode/cathode microbial fuel cells (MAC MFCs) to enhance the power production in wastewater treatment, Int. J. Hydrogen Energy. 36 (2011) 876–884. doi:10.1016/j.ijhydene.2010.08.074.

[56] S. Babu, R. Thanneeru, T. Inerbaev, R. Day, A.E. Masunov, A. Schulte, S. Seal, Dopant-mediated oxygen vacancy tuning in ceria nanoparticles, Nanotechnology. 20 (2009) 085713. doi:10.1088/0957-4484/20/8/085713.

[57] S. Tsunekawa, T. Fukuda, A. Kasuya, X-ray photoelectron spectroscopy of monodisperse CeO2−x nanoparticles, Surf. Sci. 457 (2000) L437–L440. doi:10.1016/S0039-6028(00)00470-2.

[58] F. Esch, S. Fabris, L. Zhou, T. Montini, C. Africh, P. Fornasiero, G. Comelli, R. Rosei, Electron Localization Determines Defect Formation on Ceria Substrates, Science (80-.). 309 (2005) 752–755. doi:10.1126/science.1111568.

[59] J. Paier, C. Penschke, J. Sauer, Oxygen Defects and Surface Chemistry of Ceria: Quantum Chemical Studies Compared to Experiment, Chem. Rev. 113 (2013) 3949–3985. doi:10.1021/cr3004949.

Figure captions

Figure 1 SEM micrographs of the carbon-based cathodes doped with CeO_2 nanoparticles (A, C) and with Sm-CeO_2 nanoparticles (B, D).

Figure 2. BET N_2 adsorption/desorption isotherms of CeO_2 and Sm-CeO_2 samples (A). Pore area distribution (B).

Figure 3. ORR cathodic polarization curves recorded in air-saturated carbonate buffer (A) and air-saturated 0.1 M KOH (B). T = 25 °C, v = 5 mV s^{-1}.

Figure 4. Current density (A), pH (B), anode OCP (C) and cathode OCP (D) trends of the operated MFCs during feed cycles: Sm-CeO_2 MFC (red), CeO_2 MFC (green) and control MFC (grey).

Figure 5. SEM micrographs of the CeO_2 cathode at the end of the test and EDS element analyses in two points. A): biofilm Surface; B): CeO_2 particles colonized by biofilm; C): carbonates particles growing in the cathode under the biofilm; D): EDS analysis of CeO_2 aggregates on the surface in B (d); E): EDS analysis of the carbonates in C (e).

Figure 6. (A) Cathode polarization curves and (B) power density curves performed on operating MFCs at the beginning (time 0 and acclimation), cycle 1 and cycle 3 of feeding cycles: Sm-CeO_2 MFC (red), CeO_2 MFC (green) and control MFC (grey).

Table captions

Table 1. Coulombic efficiencies for each feed-batch cycle.

Table(1)

	% Coulombic Efficiency				
	Acclimation	**Cycle 1**	**Cycle 2**	**Cycle 3**	**Cycle 4**
Control MFC	4.4	6.3	7.1	10.2	13.3
CeO_2-MFC	8.6	9.4	15.2	17.0	9.4
Sm/CeO_2-MFC	8.6	14.2	18.1	22.2	23.0

Table 1. Columbic efficiencies for each feed-batch cycle.

Figure(1)

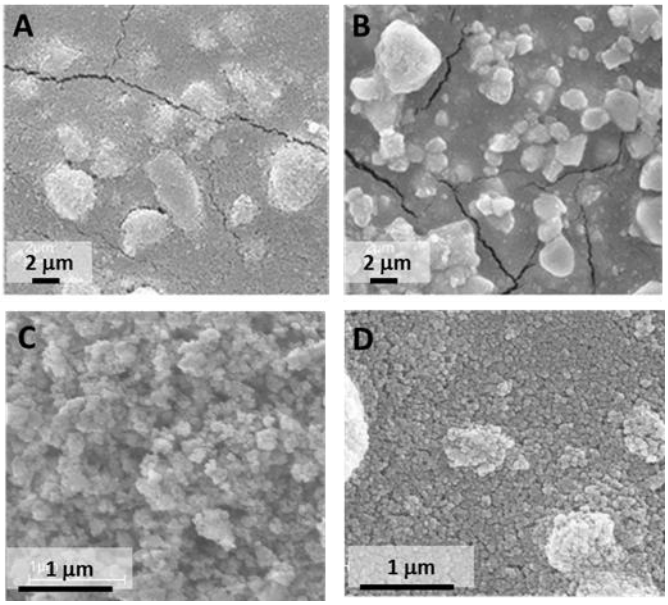

Figure(2)

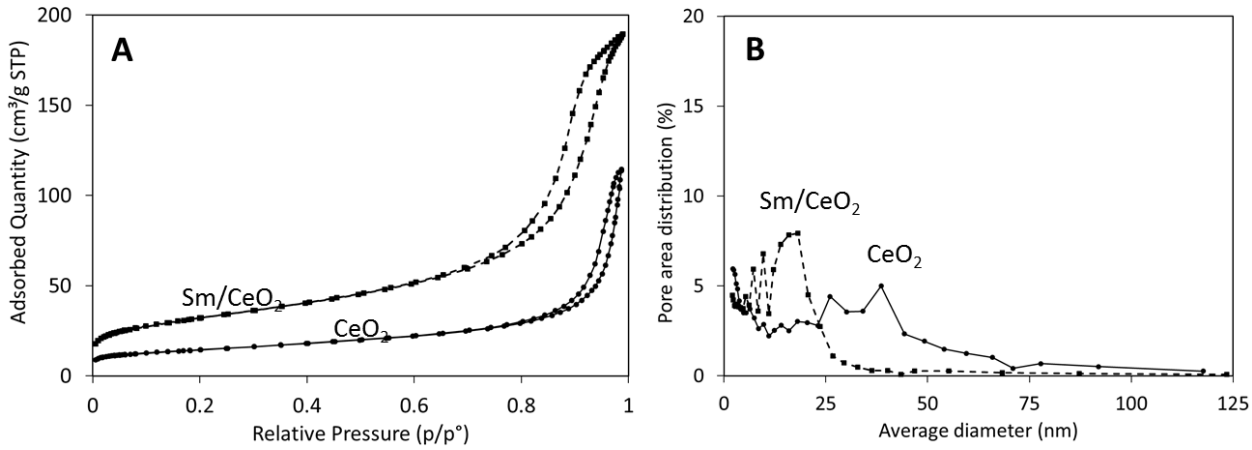

Figure 2. (A) BET N_2 adsorption/desorption isotherms of CeO_2 and Sm-CeO_2 samples. (B) Pore area distribution.

Figure(3)

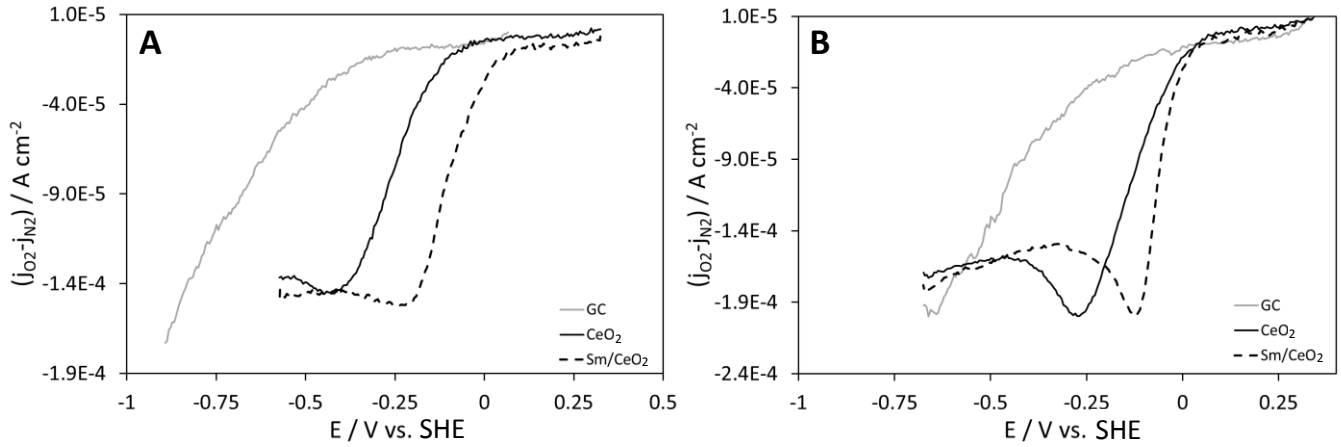

Figure 3. ORR cathodic polarization curves recorded in air-saturated carbonate buffer (A) and air-saturated 0.1 M KOH (B). T = 25 °C, ν = 5 mV s^{-1}.

Figure(4)

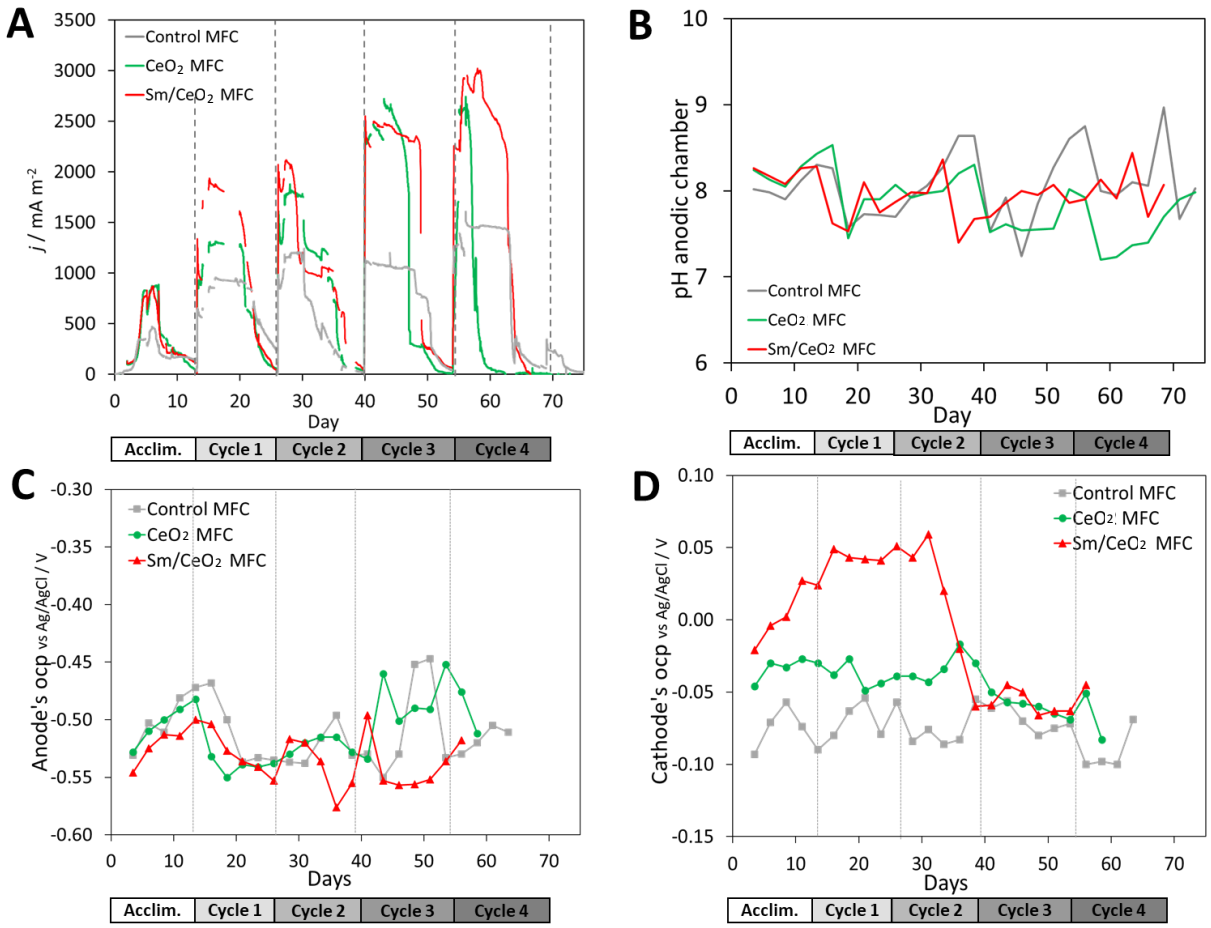

Figure 4. Current density (A), anodic chamber pH (B), anode's OCP (C) and cathode's OCP (D) trends of the operated MFCs during feed cycles: Sm-CeO_2 MFC (red), CeO_2 MFC (green) and control MFC (grey).

Figure(5)

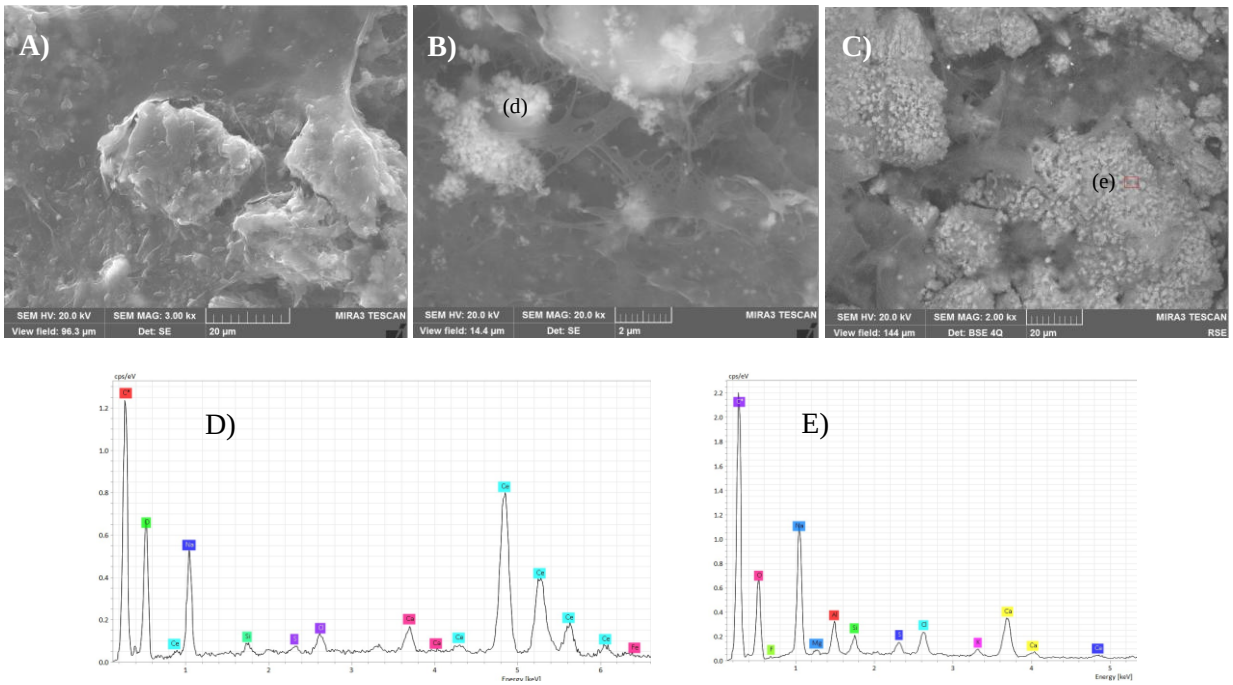

Figure 5. SEM micrographs of the CeO_2 cathode at the end of the test and EDS element analyses in two points. A): biofilm Surface; B): CeO_2 particles colonized by biofilm; C): carbonates particles growing in the cathode under the biofilm; D): EDS analysis of CeO_2 aggregates on the surface labelled (d); E): EDS analysis of the carbonates in (e).

Figure(6)

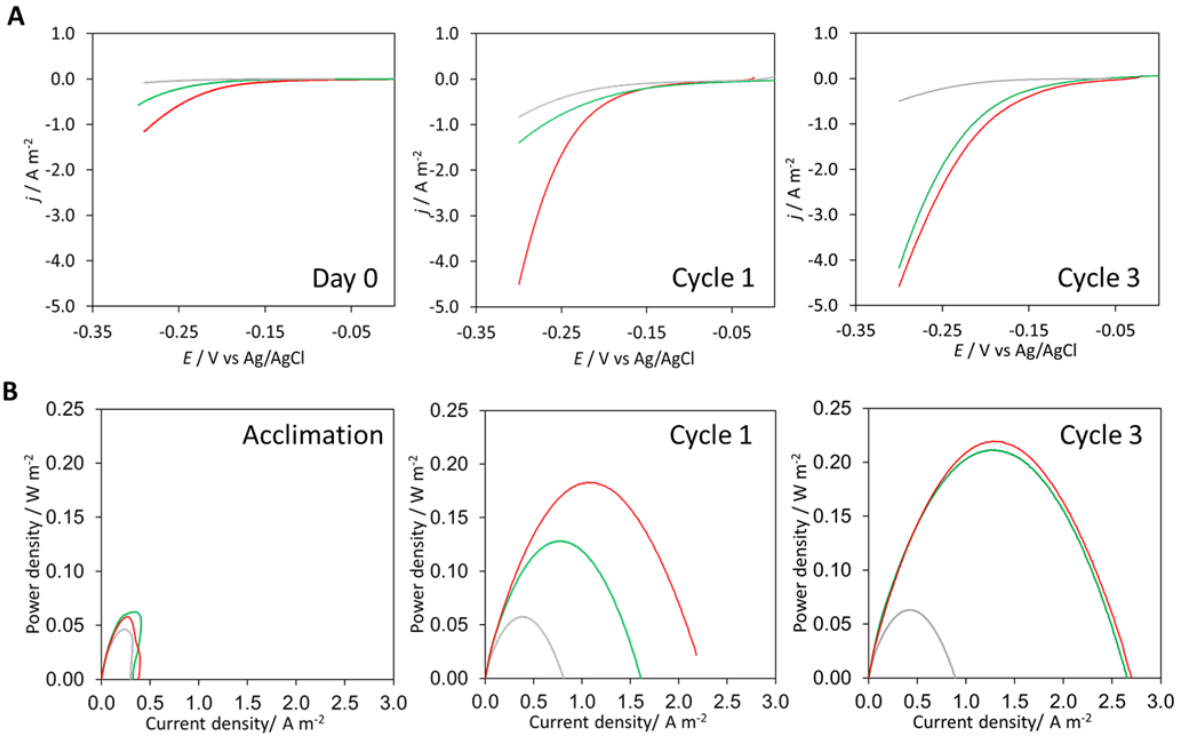
A
1.0
0.0
-1.0
-2.0
-3.0
-4.0
-5.0
j / A m-2
Day 0
Cycle 1
Cycle 3
-0.35
-0.25
-0.15
-0.05
E / V vs Ag/AgCl
B
0.25
0.20
0.15
0.10
0.05
0.00
Power density / W m-2
Acclimation
Cycle 1
Cycle 3
0.0
0.5
1.0
1.5
2.0
2.5
3.0
Current density/ A m-2

Supplementary Materials

Click here to download Supplementary Materials: Supplementary material.docx